



UNIVERSITY OF LEEDS

This is a repository copy of *Assessment of impact breakage of carbamazepine dihydrate due to aerodynamic dispersion*.

White Rose Research Online URL for this paper:
<http://eprints.whiterose.ac.uk/154034/>

Version: Accepted Version

Article:

Pin Goh, W, Ali, M, Sinha, K et al. (5 more authors) (2019) Assessment of impact breakage of carbamazepine dihydrate due to aerodynamic dispersion. *International Journal of Pharmaceutics*, 572. 118780. ISSN 0378-5173

<https://doi.org/10.1016/j.ijpharm.2019.118780>

© 2019, Elsevier. This manuscript version is made available under the CC-BY-NC-ND 4.0 license <http://creativecommons.org/licenses/by-nc-nd/4.0/>.

Reuse

This article is distributed under the terms of the Creative Commons Attribution-NonCommercial-NoDerivs (CC BY-NC-ND) licence. This licence only allows you to download this work and share it with others as long as you credit the authors, but you can't change the article in any way or use it commercially. More information and the full terms of the licence here: <https://creativecommons.org/licenses/>

Takedown

If you consider content in White Rose Research Online to be in breach of UK law, please notify us by emailing eprints@whiterose.ac.uk including the URL of the record and the reason for the withdrawal request.



eprints@whiterose.ac.uk
<https://eprints.whiterose.ac.uk/>

1 **Assessment of Impact Breakage of Carbamazepine Dihydrate due to**

2 **Aerodynamic Dispersion**

3 Wei Pin Goh^{*}, Muzammil Ali^{*}, Kushal Sinha[†], Nandkishor K. Nere[†], Raimundo Ho[†],
4 Shailendra Bordawekar[†], Ahmad Sheikh[†] and Mojtaba Ghadiri^{*}
5

6 ^{*}School of Chemical and Process Engineering, University of Leeds, Leeds, LS2 9JT, UK

7 [†]Process Research and Development, AbbVie Inc., 1 North Waukegan Road, North Chicago, Illinois, 60064, US

8 **Abstract**

9 Acicular crystals are very common in pharmaceutical manufacturing. They are very
10 prone to breakage, causing unwanted particle size degradation and problems such as
11 segregation and lump formation. We investigate the breakage pattern of carbamazepine
12 dihydrate, an acicular and platy crystal with cleavage planes. It readily undergoes attrition
13 during isolation and drying stage, causing processing difficulties. We use the aerodynamic
14 dispersion of a very small quantity of powder sample to induce breakage by applying a pulse
15 of pressurised air. The dispersion unit of Morphologi G3 is used for this purpose. The broken
16 particles settle in a chamber and are subsequently analysed using the built-in image analysis
17 software. The shift in the particle size and shape distributions is quantified through which the
18 extent of breakage is determined as a function of the dispersion pressure. The analysis reveals
19 a change of breakage mechanism as the dispersion pressure is increased from primarily
20 snapping along the crystal length to one in which chipping has also a notable contribution. The
21 breakage data are analysed using a modified impact-based breakage model and the breakability
22 index of the carbamazepine dihydrate is determined for the two breakage regimes. The method
23 provides a quick and easy testing of particle breakability, a useful tool for assessing attrition in
24 process plant and grindability in milling operations.

25 Keywords: Acicular, Breakability, Impact, Crystals, Aerodynamic Dispersion, Morphologi G3

1 Notation

Symbol Definition and units

A_d	Projected area of debris [m^2]
A_f	Projected area of feed particles [m^2]
AR	Aspect ratio [-]
B	Particle size distribution of interest [-]
B_{ref}	Reference particle size distribution [-]
D_v	Square equivalent side length (volumetric) [m]
H	Hardness [Pa]
i	Bin number [-]
K_C	Fracture toughness [$Pa \cdot m^{0.5}$]
L_v	Particle Length (volumetric) [m]
M_d	Mass of debris [kg]
M_f	Mass of feed [kg]
R^*	Extent of breakage [-]
S	Difference in area percentage of bin number j [%]
U	Normal impact velocity [m/s]
V_d	Particle volume of debris [m^3]
V_f	Particle volume of feed [m^3]
W_v	Particle Width (volumetric) [m]
α	Proportionality constant [-]
β	Breakability index [-]
ρ	Particle Density [$kg \cdot m^{-3}$]
ϕ	Volume fraction of particles [-]

1 **1 Introduction**

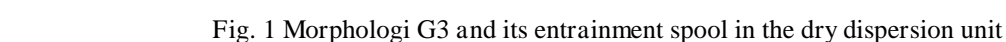
2 Active pharmaceutical ingredients (APIs) are generally crystallised for stability and
3 purity considerations, but are very often milled to obtain desired characteristics that are
4 essential for further downstream processing, such as bioavailability of the drug, compactability
5 and tableability (Rowe, 2006). Particle breakage could also be unintentional, such as the
6 particle attrition during filtration, drying, storage and transportation in the case of weak crystals,
7 which eventually leads to the degradation of product quality and handling issues. Breakage of
8 particulate solids is the result of complex interactions of material properties, environmental
9 conditions and mode of application of mechanical stresses (Tavares, 2007). A plethora of
10 works have been reported in the literature for both brittle and semi-brittle failure modes. A
11 material can exhibit both brittle and semi-brittle like behaviour depending on the strain rate.
12 Generally, increasing the strain rate can transform the failure mode from semi-brittle to brittle
13 mode. The mode of failure is also particle size dependent, where the failure mode could
14 undergo transition from brittle to semi-brittle and eventually to ductile as the size is reduced
15 (Ghadiri, 2006). Breakage of materials failing in the brittle mode is commonly analysed using
16 Weibull probability distribution (Weibull, 1951), where the breakage probability is related to
17 the applied stress and two fitting parameters that represent flaw density and material strength.
18 Vogel and Peukert (2003) applied Weibull's analysis to predict the probability of particle
19 breakage due to impact by using the approach proposed by Weichert (1988) for accounting for
20 particle size and incident kinetic energy. The breakage model developed by (Tavares and King,
21 1998) gives a distribution of the fracture probability in the log-normal form instead of
22 Weibull's distribution and is a function of the relative impact energy, the median particle
23 specific fracture energy and the geometric variance of the distribution. Both of these models
24 predict the probability of a particle to break.

1 For solids failing in the semi-brittle mode, crack initiation and propagation is preceded
2 by plastic deformation, the extent of which influences the crack features. In this case, the
3 breakage behaviour of particles is governed by their mechanical properties such as fracture
4 toughness, K_{IC} , hardness, H and Young's modulus, E (Ghadiri, 2006). Moreover, for the case
5 of organic crystals, these properties are strain-rate and temperature dependent (Duncan-Hewitt
6 and Weatherly, 1989; Hassanpour et al., 2004; Olusanmi et al., 2010). The ratio of hardness,
7 H , to fracture toughness, K_{IC} is proposed by Lawn and Marshall (1979) as a measure of the
8 brittleness of material under quasi-static indentation. Under dynamic impact loading conditions,
9 the particle breakage propensity is described by the ratio H/K_{IC}^2 (Ghadiri and Zhang, 2002).

10 Crystalline materials readily break by fracture on cleavage and slip planes (if present),
11 and/or on planes influenced by the tensile and shear stress fields. This situation is often
12 exacerbated in the case of acicular crystal shape, which is the subject of study here. Breakage
13 on cleavage planes produces smooth surfaces, whilst on other planes it is often associated with
14 uneven and irregular fracture surfaces (Klein et al., 1985). Cleavage planes have low fracture
15 surface energy and are therefore weaker than other planes within the structure. Consequently,
16 they are more prone to failure compared to the others. Good examples are sodium chloride, a
17 simple cubic crystal system which is known to readily cleave on the (100) planes (Pratt, 1953)
18 and aspirin, which also cracks preferentially on cleavage planes (100) under both quasi-static
19 and impact loading conditions, even though the cracks originate from plastically-deformed
20 regions (Olusanmi et al., 2011). Generally speaking, crystals with cleavage planes tend to break
21 into bigger fragments under the same stressing energy. In contrast, for particles with no
22 cleavage plane, a higher energy is needed to extend the cracks and hence the breakage progeny
23 is smaller in size.

24 The focus of this paper is on the breakage of acicular crystals of carbamazepine dihydrate
25 under impact loading. The mechanistic model of particle impact breakage of Ghadiri and

1 Zhang (2002) is used in this work to analyse the breakage. Morphologi G3 of Malvern
2 Panalytical Ltd, Malvern, UK, a particle size analyser based on static optical imaging analysis
3 technique, is used to assess the breakage of carbamazepine dihydrate crystals under impact
4 loading. The impact energy comes from the dry dispersion unit of the device (Fig. 1), where a
5 pulse of pressurised air is applied, by which the particles in the sample well are dispersed and
6 impact on to the internal walls of the spool before settling down onto a glass slide for
7 subsequent size and shape analysis.

8  Fig. 1 Morphologi G3 and its entrainment spool in the dry dispersion unit

9 The transient fluid flow field is calculated by CFD modelling using Fluent. The particle
10 trajectories are calculated using the same approach as of Ali and Ghadiri (2017) by adopting a
11 Lagrangian method of calculation of particle velocity. The correlation of Ganser (1993) is used
12 to account for the effect of particle shape on the fluid drag. The particle size is measured and
13 the shift in its distribution is then used following the approach of Bonakdar et al. (2016) to
14 estimate the breakability. In addition, the length and width of the particles are measured to
15 reveal the breakage mechanism in connection with the cleavage plane present in the crystal
16 lattice structure.

17 **2 Materials and Methods**

18 **2.1 Carbamazepine Dihydrate Crystals**

19 Carbamazepine dihydrate ($C_{15}H_{16}N_2O_3$) is a crystalline API that is primarily used as an
20 anticonvulsant to treat epilepsy and neuropathic pain. The crystals used in this work are
21 prepared by forward addition of anti-solvent (water) into carbamazepine-ethanol solution in a
22 10 L reactor. Anhydrous carbamazepine is first charged to a crystalliser, followed by a mixture
23 of ethanol:water (80:20 w/w%). The solution is then stirred at 250 RPM at 65 °C for complete
24 dissolution. The temperature is then reduced and wet-milled seeds of carbamazepine dihydrate

1 are added into the solution at 41 °C. Anti-solvent (water) is then charged into the solution. Two
2 heating and cooling cycles are then performed with the cooling rates of at 0.1 °C/min and
3 0.05 °C/min, respectively. The slurry is then filtered and washed twice before being subjected
4 to drying at room temperature. The crystal structure contains two water molecules, forming
5 channels of water molecules along the largest dimension of the macroscopic crystal, parallel to
6 the crystal axis c (Fig. 2). Its structure is monoclinic with a space group $P2_1/c$ (Harris et al.,
7 2005). It is acicular and platy, owing to the fact that the growth rate of the first two dimensions
8 which constitute the dominant faces (h00) and (0k0) of the crystals is substantially higher than
9 the third dimension (Fig. 3a). Crystal axes b and c correspond to the particle length and width
10 of the grown crystals. The orderly arrangement of water channels in the lattice structure leads
11 to the formation of cleavage planes (0k0) that are perpendicular to the dominant face (h00) of
12 the crystal. These planes are very weak and are known to get exposed easily upon dehydration
13 due to stress relief (Khoo et al., 2013). The formation of cracks on h00 face is shown in Fig.
14 3b. They are parallel to the crystal axis c as a result of detachment of water molecule from the
15 crystal lattice channels (Rauber, 2018). Polarised micrographs of the crystals are reproduced
16 from Rauber (2018) in Fig. 3c, showing the quality of the crystals. The water content of the
17 crystals is around 13%, as determined by Thermogravimetric Analysis and is in line with the
18 theoretical water content of carbamazepine dihydrate (13.2%).

19 Fig. 2 Calculated Bravais, Friedel, Donnay and Harker (BFDH) crystal morphology of carbamazepine
20 dihydrate

21 Fig. 3 (a) Carbamazepine dihydrate crystals viewed by scanning electron microscope (SEM); (b) Formation of
22 cracks on weak cleavage planes along h00 face under vacuum in the SEM chamber due to dehydration; (c)
23 Polarised micrographs of the carbamazepine dihydrate crystals (Rauber, 2018).

24

1 2.2 Experimental Setup

2 A small amount of sample ($\sim 5 \text{ mm}^3$) is first placed into the dispersion spool of the dry
3 dispersion unit of Morphologi G3. A pulse of pressurised air is then applied to disperse the
4 particles, as a result of which they impact against the internal walls of the spool and possibly
5 break before they exit the disperser and settle down onto the glass slide inside the collection
6 chamber. The dispersion pressures used in this work range from 0.5 barg to 5 barg (with 0.5
7 barg interval between the consecutive tests). Six samples are used for each dispersion pressure
8 to ensure that adequate population of particles is analysed. A series of grayscale images
9 covering the whole scan area are captured by the microscope unit of the device with the aids
10 of the automated XYZ stage under episcopic lighting condition. Image thresholding is
11 performed to convert the grayscale images into binary images and isolate the particles from the
12 background. The individual particle morphological properties are then analysed using the built-
13 in image analysis suite. The lens selected is of $5\times$ magnification and particles captured with
14 less than 10 pixels are not considered in the size and shape analysis.

15 2.3 Exclusion of Particle Anomaly by Image Analysis

16 A series of tests were performed initially to determine the optimal sample size, which has
17 the largest particle population while attaining the minimum occurrence of particle overlaps.
18 Nevertheless, there still existed some particles that laid on top of each other, appearing as a
19 clump of particles (Fig. 4). If left unattended, these will be treated as single particles in the
20 image analysis, leading to false representations of the particle size and shape distribution, hence
21 causing errors in the breakage analysis. Filters based on particle convexity and solidity are
22 applied to remove them. These shape parameters give an indirect measure of the “spikiness”
23 of the particle. A clump that is made up of multiple particles will appear to be more spiky than
24 individual crystal. A sensitivity analysis was performed to determine the optimal values for

1 convexity and solidity, and it was found that a value of 0.85 used for both parameters filtered
2 out most of the overlapping particles while keeping the individual particles intact.

3 Fig. 4 Clumps of carbamazepine dihydrate crystals

4 2.4 Particle Volume Estimation

5 Like most particle analysers, Morphologi G3 captures 2-dimensional information of the
6 particles, as they lie on their maximum stable plane. Carbamazepine dihydrate crystals are platy
7 and their third dimension is significantly smaller than the other two dimensions. Therefore, the
8 volumetric particle size distribution is calculated based on the crystal projected area, assuming
9 constant thickness.

10 2.5 Statistical Reliability and Data Smoothing

11 Particle size and shape analysis by G3 Morphologi uses a miniscule sample, typically in
12 milligram range for each measurement. However, a small sample size is also associated with
13 lower population of particles being measured and hence the particle size distribution may not
14 be fully representative. Depending on the particle size and shape of the sample, multiple
15 measurements may have to be performed to improve the statistical reliability of the measured
16 particle size distribution. The particle size distribution of bigger and non-spherical particles,
17 especially those with large aspect ratio, tends to have a wider scatter compared to those of
18 smaller and rounded ones. The particle size distribution measured using G3 Morphologi is in
19 the form of discrete probability distribution but is presented here as continuous probability
20 distribution for better visual presentation. The scatter of the PSD is large for each individual
21 measurement (~20000 particles), summing these measurements from six samples reduces the
22 scatter considerably, but not to a desirable level. Undoubtedly, increasing the number of
23 measurements will eventually smoothen out these peaks but doing so would defy the whole
24 purpose of using the G3 Morphologi as a quick alternative for particle morphology

1 measurement technique. Therefore, a simple moving average (SMA) of 11 points from
2 successive bins of the particle size distributions is calculated to iron out the peaks present due
3 to the deficiency of particle population in the measurement. The optimal number of points is
4 determined based on the criterion that the smoothed plot remains within the scatter of the
5 original plot. As shown in Fig. 5, a moving average of 11 points produces a reasonably
6 smoothed plot and the overall distribution is not shifted excessively.

7 Fig. 5 Moving average of PSD using different number of points

8 **3 Impact Velocity Prediction by Computational Fluid Dynamics (CFD)**

9 Prediction of impact velocity of particles is carried out using transient three-dimensional
10 CFD modelling of G3 Morphologi disperser to take into account the effect of air flow and
11 turbulence on the trajectories of particles. Commercial CFD software Ansys Fluent (2017) is
12 used to solve the continuous (air) phase flow equations. To assess the impact of inlet pressure
13 pulse on the impact velocities of particles, the simulation is carried out using inlet air pressures
14 of 0.5 to 5 barg in 0.5 barg progression. Each simulation is run at the specified inlet pressure
15 for 20 ms, thereafter the pulse is stopped by changing the pressure to 0 barg. The simulation is
16 allowed to run until all the particles exit the domain. Details of the CFD modelling
17 methodology, numerical solution method and the mesh used in the CFD simulations can be
18 found in an earlier work carried out by Ali and Ghadiri (2017) in which triboelectric charging
19 of particles in G3 disperser was studied using CFD modelling.

20 **3.1 Modelling of particle trajectories**

21 The discrete phase is considered to comprise thin cuboid shape particles with constant
22 width and thickness of 100 μm and 20 μm , respectively and length of 100, 250, 500 and 1000
23 μm . The density of particles is considered to be constant with a value of 1270 kg/m^3 . The
24 particles are initially placed in the sample well and dispersed by a pulse of pressurised air. The

1 trajectories of particles are computed by solving the equation of motion of particles considering
2 the drag and gravitational forces. For these particles shapes, the drag coefficient is calculated
3 using correlations given by Ganser (1993). The rotation of particles is not considered. One-
4 way coupling is assumed between the particles and the air, i.e. the air flow influences the
5 trajectories of particles, but the momentum exerted by the particles on the air is ignored. The
6 interaction between the particles is also not considered. The maximum impact velocity of
7 particles in the disperser takes place at the wall just above the sample well (Fig. 1). For the
8 purpose of predicting the impact velocity, the velocity of particles colliding with this region of
9 the wall is recorded and the impacted particle is eliminated from the computational domain. To
10 get a statistically representative impact velocity, 1000 particles are tracked for each size and
11 the average value is used.

12

13 **4 Experimental Results and Discussions**

14 4.1 Size Reduction of Carbamazepine Dihydrate Crystals

15 The averaged PSDs of carbamazepine dihydrate at different dispersion pressures are
16 shown in Fig. 6a. Gradual shifting of the size distribution to the left is observed as the
17 dispersion pressure is increased. The reduction in the number of the larger particles indicates
18 that the particle breakage is dominated by fragmentation upon dispersion. Extensive breakage
19 is observed above 4 barg pressure. The characteristic sizes, $D_{V,10}$, $D_{V,50}$ and $D_{V,90}$ are determined
20 from the cumulative volume plots of these distributions (not shown in this paper) and the
21 relationship between these attributes and the dispersion pressure is depicted in Fig. 6 (b). The
22 subscript that follows after D_V is the volume percentage below the size of interest. It can be
23 seen that the $D_{V,90}$ value at 5 barg, the highest dispersion pressure tested, is almost half of the
24 one at 0.5 barg, indicating a reduction in particle volume by approximately a factor of four

1 (assuming 2D dominant shape of the crystal). $D_{v,10}$ on the other hand shows that the volume of
 2 the smaller particles at 5 barg is ~140 times smaller than those at 0.5 barg, indicating the
 3 particles undergo a significant size reduction upon being dispersed at 5.0 barg.

4 Fig. 6 (a) Particle size distribution of carbamazepine dihydrate crystals dispersed at different pressures; (b)
 5 Characteristic volumetric intercept values of square equivalent side length, $D_{v,10}$, $D_{v,50}$ and $D_{v,90}$

6 4.2 Extent of Breakage

7 The extent of breakage, R^* gives a measure of the amount of debris produced after a
 8 breakage event, normally expressed on gravimetric basis, given by Eq. 1. This gravimetric ratio
 9 can be converted to volumetric ratio as the density is the same for all the particles.

$$R^* = \frac{M_d}{M_f} = \frac{V_d}{V_f} \quad (1)$$

10 where M_d is the mass of debris, M_f is the mass of feed, V_d and V_f are the cumulative particle
 11 volumes (not the bulk volume) of debris, and the feed, respectively. This relationship can
 12 further be simplified and expressed as a ratio of projected areas if the thickness is considered
 13 constant for all sizes:

$$R^* = \frac{M_d}{M_f} = \frac{V_d}{V_f} = \frac{A_d}{A_f} \quad (2)$$

14 where A_d the projected area of debris and A_f the projected area of feed particles. A_d/A_f can be
 15 obtained by subtracting the reference PSD (subjected to the lowest dispersion pressure, 0.5
 16 barg) from the PSD of interest. It is noteworthy that the pressure pulse of 0.5 barg does not
 17 break the particle to any notable extent, as the wet analysis (i.e. dispersing the particles in a
 18 liquid carrier) produces almost the same size distribution. The integral of the positive difference
 19 as illustrated in Fig. 7 can be calculated using Eqs 3 and 4.

$$S_i = B_i - B_{\text{ref},i} \quad (3)$$

$$R^* = \sum_{i=1}^n S_i [S_i > 0] \quad (4)$$

1 where S_i is the difference between the area percentage of the reference PSD, $B_{\text{ref},i}$ and the PSD
 2 of broken particles, B_i in the bin number i and R^* the sum of the positive differences between
 3 the two PSDs up to bin number n (the particle size is segmented into 1001 bins in the
 4 Morphologi G3, maximum particle size being 2 mm). The extent of breakage of carbamazepine
 5 dihydrate crystals as a function of the dispersion pressure is illustrated in Fig. 8. The data points
 6 presented are the mean extent of breakage calculated from the six repeated samples and the
 7 vertical bars being the standard deviation (SD). It can clearly be seen that as the dispersion
 8 pressure increases, the extent of breakage increases too. The extent of breakage does not
 9 increase linearly with the dispersion pressure. This could be attributed to the fact that the
 10 particles have a limited travel distance in the dispersion spool to accelerate before impacting
 11 on the wall and hence increasing the dispersion pressure does not increase the impact velocity
 12 much at higher pressure.

13 It is evident that the particles break more as the dispersion pressure increases, though at
 14 lower dispersion pressures (below 2 barg), an increase in the extent of breakage is more
 15 prominent. The extent of breakage is in the range from 20% at 1 barg up to 60% at 5 barg with
 16 respect to the reference size distribution measured at 0.5 barg. This observation agrees very
 17 well with the qualitative comparison of the PSDs and quantitative investigation of
 18 characteristic sizes discussed in the previous section, which further stipulates that the
 19 carbamazepine dihydrate crystals are highly prone to breakage upon dispersion.

20 Fig. 7 Calculation of R^* in the form of A_b/A_r (%)

21 Fig. 8 Extent of breakage of carbamazepine dihydrate crystals at different dispersion pressures

1 The mode of breakage of carbamazepine dihydrate is very different compared to that of
2 equant particles. High aspect ratio particles experience bending moments along their long axis
3 and could snap along the length. The presence of cleavage plane on the dominant face (h00)
4 adds to the complexity of the breakage pattern. Even though breakage on cleavage planes
5 requires low energy and is often the preferred route for crack propagation, the geometric effect
6 of the high aspect ratio of carbamazepine dihydrate could make breakage along the length more
7 dominant. Much like the volume distribution, length and width distribution of carbamazepine
8 dihydrate (not shown for brevity) widens and shifts to the left as the dispersion pressure is
9 increased. The trend of breakage of acicular particles across their largest dimension is
10 supported by the change of characteristic length, L_v at 90%. The change of particle length
11 between each pair of consecutive pressures is notable, especially at lower dispersion pressures
12 up to 2 barg, exactly similar to the equivalent side length shown in Fig. 6. Despite the presence
13 of cleavage planes that are parallel to the particle length (Rauber, 2018), carbamazepine
14 dihydrate crystals fracture across the particle length upon impact. This is a clear evidence that
15 the geometric effect of bending of carbamazepine dihydrate is of significance. Breakage across
16 its width (along planes parallel to the long axis) is also observed due to cleaving. The reduction
17 of both particle length and width takes place at a fast rate at lower pressures, but it slows down,
18 approaching an asymptotic level, as the dispersion pressure is increased. There exists a
19 transition point at around 2 barg above which the changes in particle length and width between
20 each pair of consecutive pressures become more gradual. These results show that unlike other
21 acicular crystals, such as β -glutamic acid (Saifoori et al., 2019), carbamazepine dihydrate
22 crystals do break in a noticeable degree along both their length and width. Though not to the
23 same extent as the particle length, there is a substantial reduction in the particle width from 180
24 to 100 μm (~44%). Micrograph by SEM in Fig. 9 (a) clearly shows cracks along the particle
25 length, parallel to the crystal axis c where the cleavage planes (0k0) exist. In contrast, the

1 fracture along the particle length, i.e. on planes perpendicular to axis c, has a more irregular
2 edge (Fig. 9b). This is in agreement with the crystal lattice structure of carbamazepine
3 dihydrate, as there has been no slip/cleavage plane identified perpendicular to the particle
4 length. **Error! Reference source not found.**

5 Fig. 9 Fracture of carbamazepine dihydrate crystal along its width (a) and its length (b)

6 The distributions of particle aspect ratio, defined as width over length, at different
7 dispersion pressures have also been determined, but not shown here for brevity. As the pressure
8 is increased, the shape becomes more equant, indicating that the crystals undergo a higher
9 extent of breakage along their length. The characteristic value of aspect ratio, $AR_{V,90}$ shows a
10 change with pressure, whilst $AR_{V,10}$ and $AR_{V,50}$ show little/no variations, indicating a higher
11 tendency for the larger particles to undergo size reduction and shape modification. Above 3
12 barg, the aspect ratio of the particles does not change much and remains at around 0.8. This
13 provides an explanation to the two different regimes observed from plots of particle size, length
14 and width. Initially when the particles are acicular, they undergo substantial fragmentation due
15 to the geometric effect of the particles. However, as the dispersion pressure increases, it reaches
16 a point where the particles are no longer acicular, but more equant and hence leads to a situation
17 in which chipping is also prevalent.

18 4.3 Impact Breakage Assessment of Carbamazepine Dihydrate

19 Impact is the main cause of breakage in the dispersion spool of G3 Morphologi. For
20 correlating the extent of breakage of particles and their intrinsic physical and mechanical
21 properties, the impact breakage model of Ghadiri and Zhang (2002) is used, given by Eq. 5.

$$R^* = \alpha \frac{H}{K_c^2} \rho D U^2 \quad (5)$$

1 where R^* is the extent of breakage, α the proportionality constant, H the hardness, K_C
 2 the fracture toughness, ρ the particle density, D the particle size and U the particle impact
 3 velocity. The functional group of $\alpha \frac{H}{K_C^2}$ governs the breakage propensity of a material and is
 4 known as the breakability index and could be inferred from the impact tests as shown below.

5 For highly acicular particles like carbamazepine dihydrate crystals, it is difficult to
 6 classify them into narrow size classes by length or width. Therefore, a full range of particle
 7 sizes present in the sample is used instead. The original breakage model is therefore modified
 8 so that it could accommodate the full-size distribution of the sample. The volume fraction of
 9 particles in different size classes in the original feed sample is taken into account in the
 10 modified impact breakage model and is presented below.

$$R^* = \beta \rho \sum_{i=1}^n \phi_i D_i U_i^2 \quad (6)$$

11 where β is the breakability index, ρ the particle density, i the bin number, ϕ the volume
 12 fraction of the particles, D the representative particle size, and U the corresponding particle
 13 impact velocity in the bin i .

14 The calculated impact velocities of particles with different sizes and aspect ratios in the
 15 dispersion spool at different dispersion pressures are depicted in Fig. 10. The numerical aspect
 16 of this work is detailed in section 3. The calculated particle normal impact velocity at different
 17 dispersion pressures is plotted as a function of the particle length. Interestingly, the variation
 18 of impact velocity with particle length is not notable, except for smaller particle lengths.

19 Fig. 10 Normal impact velocity of carbamazepine at different dispersion pressure as a function of particle
 20 length

1 The particle-wall impact velocities shown in Fig. 10 are used in Eq. 6 to calculate the
2 extent of breakage and the results are plotted in Fig. 11. The slope of the regression line
3 represents the breakability index of the carbamazepine dihydrate. Considering the whole data
4 set for fitting the best line by regression, the breakability index of the carbamazepine dihydrate
5 is calculated to be 0.253, with a regression coefficient of ~ 0.94. However, having one single
6 global breakability index may not be representative, as two regimes can be distinguished, as
7 discussed previously. These regimes are taken into consideration and segmented regression is
8 performed on the data instead. Fig. 11 shows the plot of R^* versus $\sum_{i=1}^n \rho DU^2$, the red broken
9 regression line corresponds to the first regime where carbamazepine crystals are snapping off
10 along their largest dimension and the broken blue regression line corresponds to the second
11 regime where particles would also break by other mechanisms. For this region, the particle
12 breakability index is smaller. The rapid breakage regime (red) has a breakability index of 0.47,
13 while the second breakage regime has a breakability index of 0.20. It should be borne in mind
14 that Ghadiri and Zhang (2002) breakage model was developed based on chipping and was not
15 tested rigorously with particles that undergo fragmentation. However, Olusanmi et al. (2011)
16 show that Ghadiri and Zhang (2002) model fits the fragmentation data of aspirin very well. The
17 model also fits the breakage data of carbamazepine dihydrate crystals that undergo rapid
18 fragmentation.

19 Fig. 11 Segmented regression of R^* versus $\sum_{i=1}^n \rho DU^2$ (normal impact)

20 **5 Conclusions**

21 A new breakability assessment technique has been used to study the extent of impact
22 breakage of acicular particles of carbamazepine dihydrate. Using the G3 Morphologi, the
23 crystals are dispersed by a pressure pulse of air, causing impact breakage. The shift of particle

1 size, length, width and aspect ratio is analysed, indicating that carbamazepine dihydrate crystals
2 tend to break along their largest dimension, due to bending arising from the geometric effect
3 of the high aspect ratio and in spite of the presence of cleavage planes. Nevertheless, breakage
4 along the crystallographic cleavage plane of weakness is also observed to a minor extent. These
5 observations suggest that the breakage of carbamazepine is dominated by both fracturing
6 perpendicular and cleaving parallel to the particle length.

7 A full particle size distribution is used in the test due to difficulty of classifying the
8 crystals in narrow size ranges. The breakability index of carbamazepine dihydrate is
9 determined by plotting the graph of R^* versus $\sum_{i=1}^n \rho DU^2$, where a non-linear relationship is
10 noted. The trend can be partitioned into two regimes, where in the first one fragmentation along
11 the crystal axis is dominant (i.e. snapping of particles along their length), whilst in the second
12 regime chipping is also prevalent. This work demonstrates that acicular crystals break easily
13 by aerodynamic dispersion and that the process can be analysed by recourse to a modified
14 impact breakage model, from which the breakage tendency could be inferred. In this way, the
15 role of crystal structure properties, particularly the existence of cleavage planes, together with
16 the effect of physical and geometric properties on the breakage behaviour of carbamazepine
17 dihydrate crystals can be studied.

18 **Disclosures:** Data were generated by the University of Leeds. AbbVie Inc., North
19 Chicago, USA, provided financial support for a studentship of Wei-Pin Goh. Kushal Sinha,
20 Nandkishor Nere, Raimundo Ho, Shailendra Bordawekar and Ahmad Sheikh are present
21 employees of AbbVie Inc.

22 **Acknowledgements**

1 The research work reported here was part of a tripartite research programme executed by
2 the Universities of Cambridge and Leeds, and Imperial College London, and financially
3 supported by AbbVie, Chicago, USA. The authors would like to thank Professor Bill Jones, Dr
4 Jerry Heng and their team members, Dr Gabriela Schneider Rauber, Dr Eftychios Hadjittofis
5 and Mr Mark-Antonin Isbell for helpful discussions. Figure 3c comes from the PhD dissertation
6 of Gabriela Schneider Rauber, who carried out polarised light microscopy on the crystals used
7 in this work for which we are grateful.

8

1 **6 References**

- 2 Ali, M. and Ghadiri, M. 2017. Analysis of triboelectric charging of particles due to
3 aerodynamic dispersion by a pulse of pressurised air jet. *Advanced Powder Technology*.
4 **28**(10),pp.2735–2740.
- 5 ANSYS® Academic Research. 2017. Ansys Fluent.
- 6 Bonakdar, T., Ali, M., Dogbe, S., Ghadiri, M. and Tinke, A. 2016. A method for grindability
7 testing using the Scirocco disperser. *International Journal of Pharmaceutics*. **501**(1–
8 2),pp.65–74.
- 9 Duncan-Hewitt, W.C. and Weatherly, G.C. 1989. Evaluating the Deformation Kinetics of
10 Sucrose Crystals Using Microindentation Techniques. *Pharmaceutical Research: An*
11 Official Journal of the American Association of Pharmaceutical Scientists.
12 **6**(12),pp.1060–1066.
- 13 Ganser, G.H. 1993. A rational approach to drag prediction of spherical and nonspherical
14 particles. *Powder Technology*. **77**(2),pp.143–152.
- 15 Ghadiri, M. 2006. Particle Impact Breakage In: H. Masuda, K. Higashitani and H. Yoshida,
16 eds. *Powder Technology Handbook*. CRC Press, pp. 205–212.
- 17 Ghadiri, M. and Zhang, Z. 2002. Impact attrition of particulate solids. Part 1: A theoretical
18 model of chipping. *Chemical Engineering Science*. **57**(17),pp.3659–3669.
- 19 Harris, R.K., Ghi, P.Y., Puschmann, H., Apperley, D.C., Griesser, U.J., Hammond, R.B., Ma,
20 C., Roberts, K.J., Pearce, G.J., Yates, J.R. and Pickard, C.J. 2005. Structural studies of the
21 polymorphs of carbamazepine, its dihydrate, and two solvates. *Organic Process Research*
22 and Development. **9**(6),pp.902–910.
- 23 Hassanpour, A., Ghadiri, M., Bentham, A.C. and Papadopoulos, D.G. 2004. Effect of

- 1 temperature on the energy utilisation in quasi-static crushing of ??-lactose monohydrate.
2 Powder Technology. **141**(3),pp.239–243.
- 3 Khoo, J.Y., Shah, U. V., Schaeperstoens, M., Williams, D.R. and Heng, J.Y.Y. 2013. Process-
4 induced phase transformation of carbamazepine dihydrate to its polymorphic anhydrides.
5 Powder Technology. **236**,pp.114–121.
- 6 Klein, C., Hurlbut, C.S. and Dana, J.D. 1985. Manual of Mineralogy 20th ed. New York: Wiley.
- 7 Lawn, B.R. and Marshall, D.B. 1979. Hardness, Toughness, and Brittleness: An Indentation
8 Analysis. Journal of the American Ceramic Society. **62**(7–8),pp.347–350.
- 9 Olusanmi, D., Roberts, K.J., Ghadiri, M. and Ding, Y. 2011. The breakage behaviour of Aspirin
10 under quasi-static indentation and single particle impact loading: Effect of
11 crystallographic anisotropy. International Journal of Pharmaceutics. **411**(1–2),pp.49–63.
- 12 Olusanmi, D., Wang, C., Ghadiri, M., Ding, Y. and Roberts, K.J. 2010. Effect of temperature
13 and humidity on the breakage behaviour of Aspirin and sucrose particles. Powder
14 Technology. **201**(3),pp.248–252.
- 15 Pratt, P.L. 1953. Cleavage deformation in zinc and sodium chloride. Acta Metallurgica.
- 16 Rauber, G. 2018. Examination of stress-induced transformations within multicomponent
17 pharmaceutical crystals.
- 18 Rowe, R. 2006. Handbook of pharmaceutical excipients. London Greyslake, IL Washington,
19 DC: Pharmaceutical Press American Pharmacists Association.
- 20 Saifoori, S., Goh, W.P., Ali, M. and Ghadiri, M. 2019. Impact Breakage of Acicular Crystals.
21 Powder Technology. In Press.
- 22 Tavares, L.. and King, R.. 1998. Single-particle fracture under impact loading. International

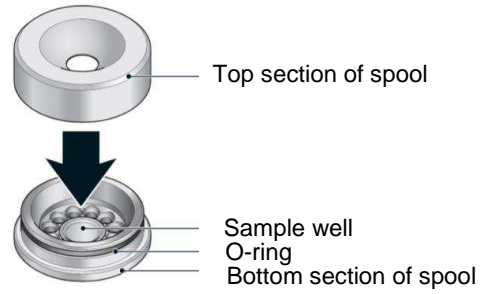
- 1 Journal of Mineral Processing. **54**(1),pp.1–28.
- 2 Tavares, L.M. 2007. Chapter 1 Breakage of Single Particles: Quasi-Static. Handbook of
3 Powder Technology. **12**(21),pp.3–68.
- 4 Vogel, L. and Peukert, W. 2003. Breakage behaviour of different materials - Construction of a
5 mastercurve for the breakage probability. Powder Technology. **129**(1–3),pp.101–110.
- 6 Weibull, W. 1951. A statistical distribution function of wide applicability. Journal of applied
7 mechanics. **18**,pp.293–297.
- 8 Weichert, R. 1988. Correlation between probability of breakage and fragment size distribution
9 of mineral particles. International Journal of Mineral Processing. **22**(1–4),pp.1–8.
- 10

1 **Figures**

Morphologi G3



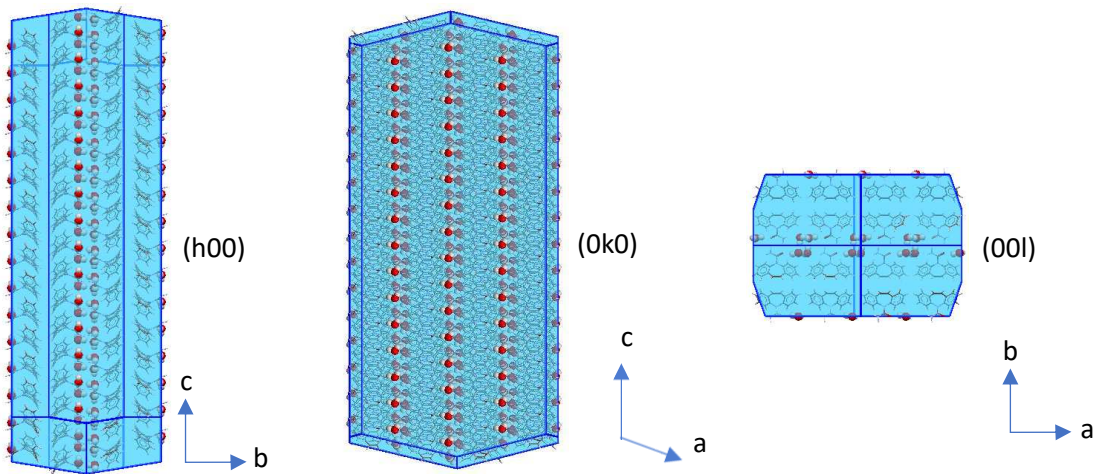
Entrainment Spool



2

3

Fig. 1 Morphologi G3 and its entrainment spool in the dry dispersion unit

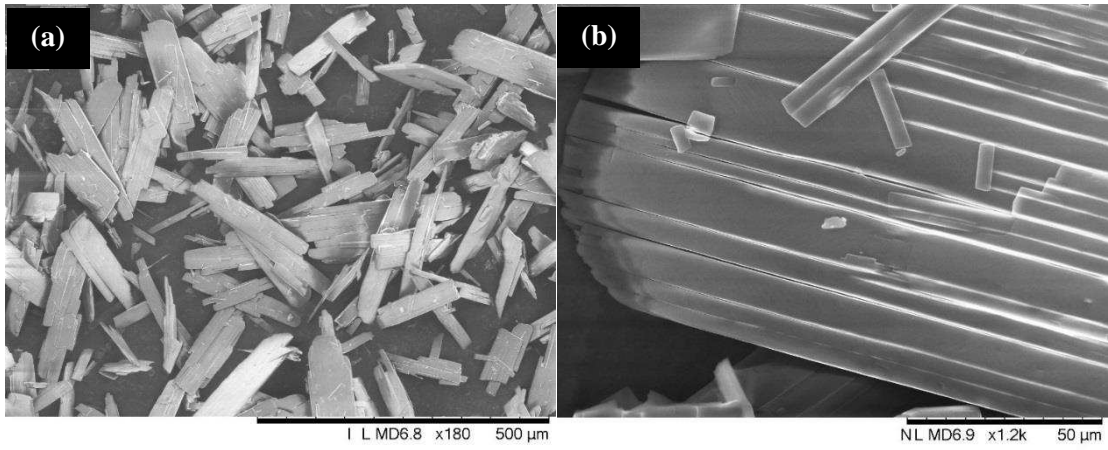


4

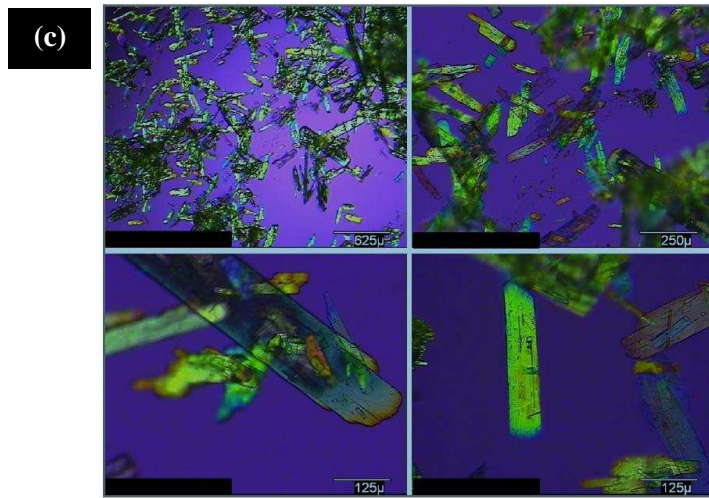
5

6

Fig. 2 Calculated Bravais, Friedel, Donnay and Harker (BFDH) crystal morphology of carbamazepine dihydrate



1



2

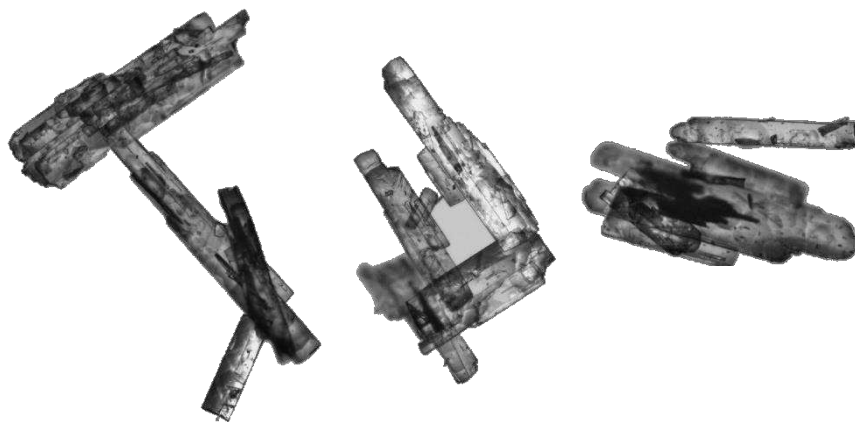
3

4

5

6

Fig. 3 (a) Carbamazepine dihydrate crystals viewed by scanning electron microscope (SEM); (b) Formation of cracks on weak cleavage planes along h00 face under vacuum in the SEM chamber due to dehydration; (c) Polarised micrographs of the carbamazepine dihydrate crystals (Rauber, 2018).



7

8

Fig. 4 Clumps of carbamazepine dihydrate crystals

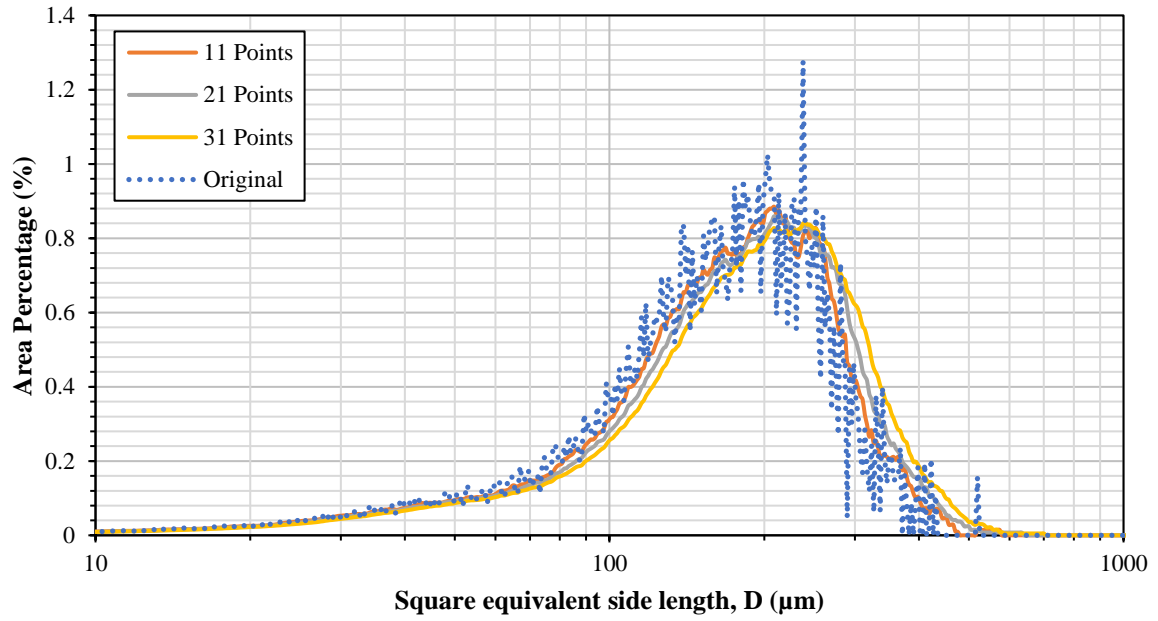
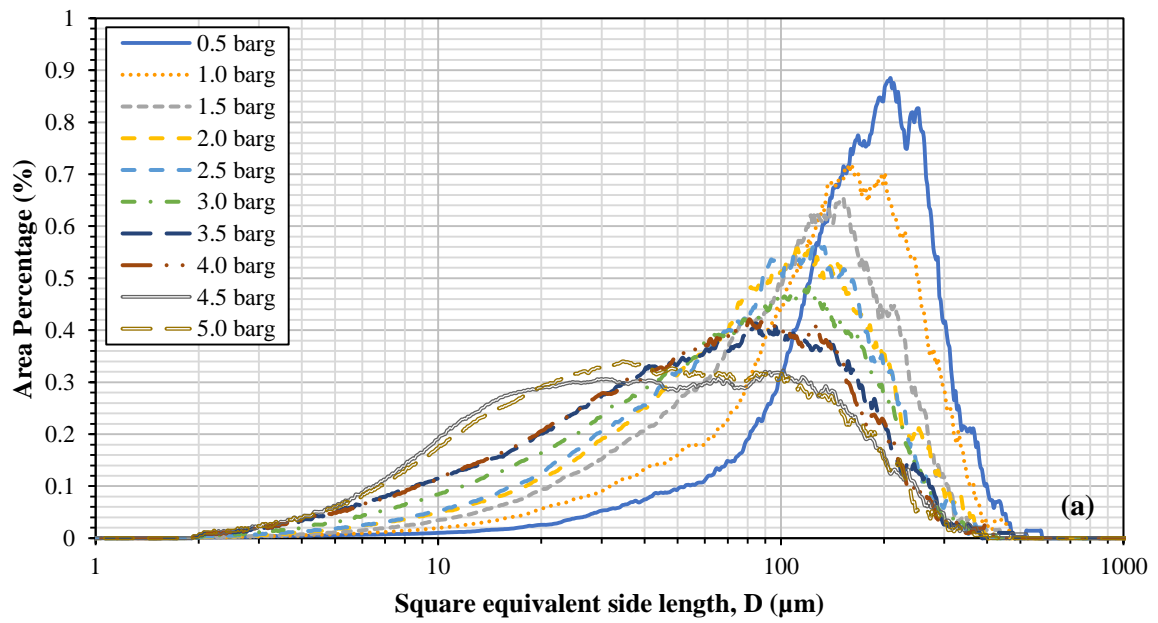
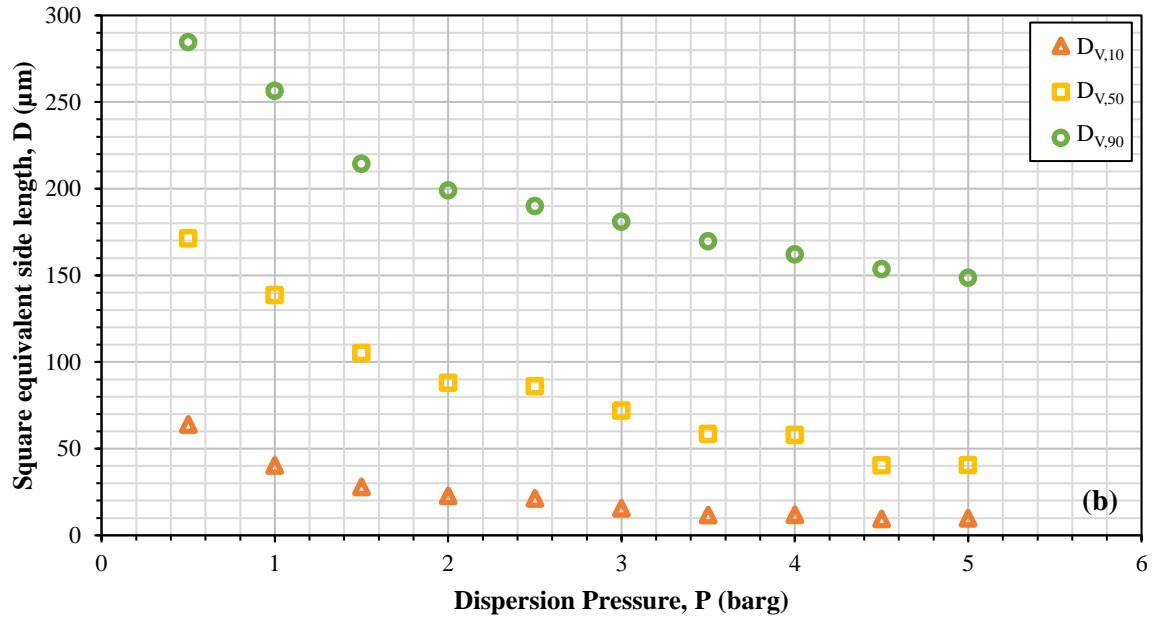


Fig. 5 Moving average of PSD using different number of points



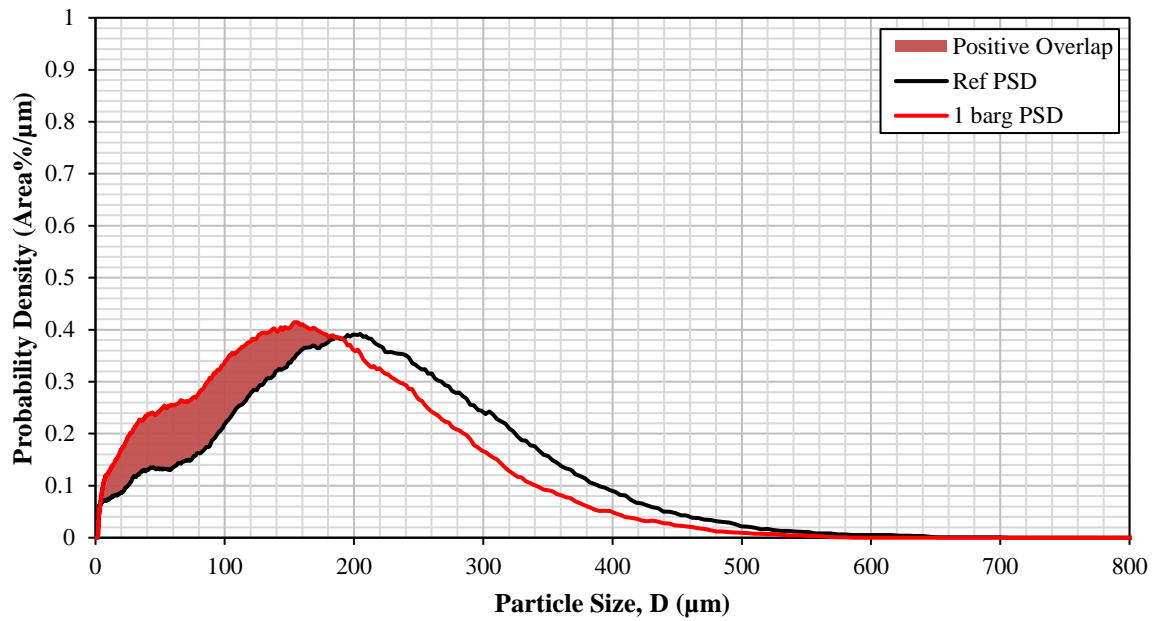


1

2

Fig. 6 (a) Particle size distribution of carbamazepine dihydrate crystals dispersed at different pressures; (b) Characteristic volumetric intercept values of square equivalent side length, $D_{v,10}$, $D_{v,50}$ and $D_{v,90}$

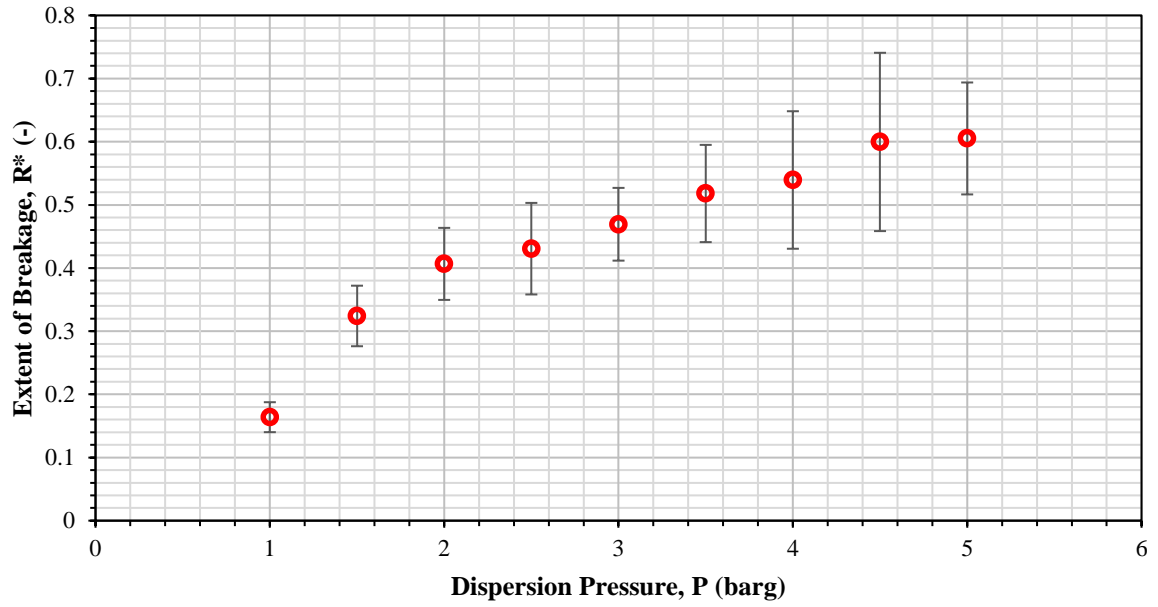
3



4

5

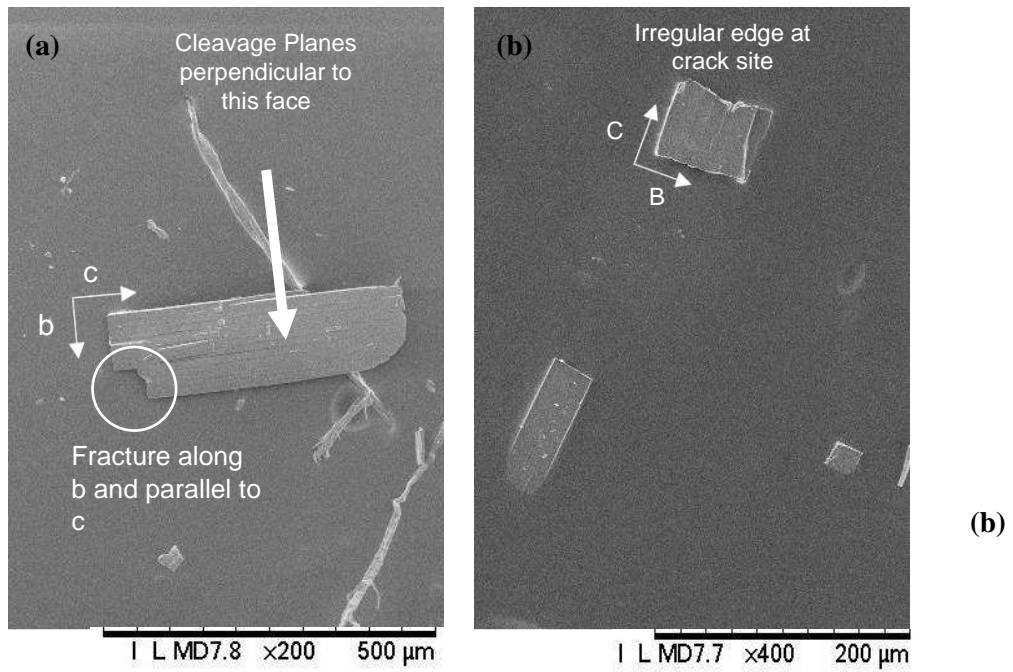
Fig. 7 Calculation of R^* in the form of A_b/A_t (%)



1

2

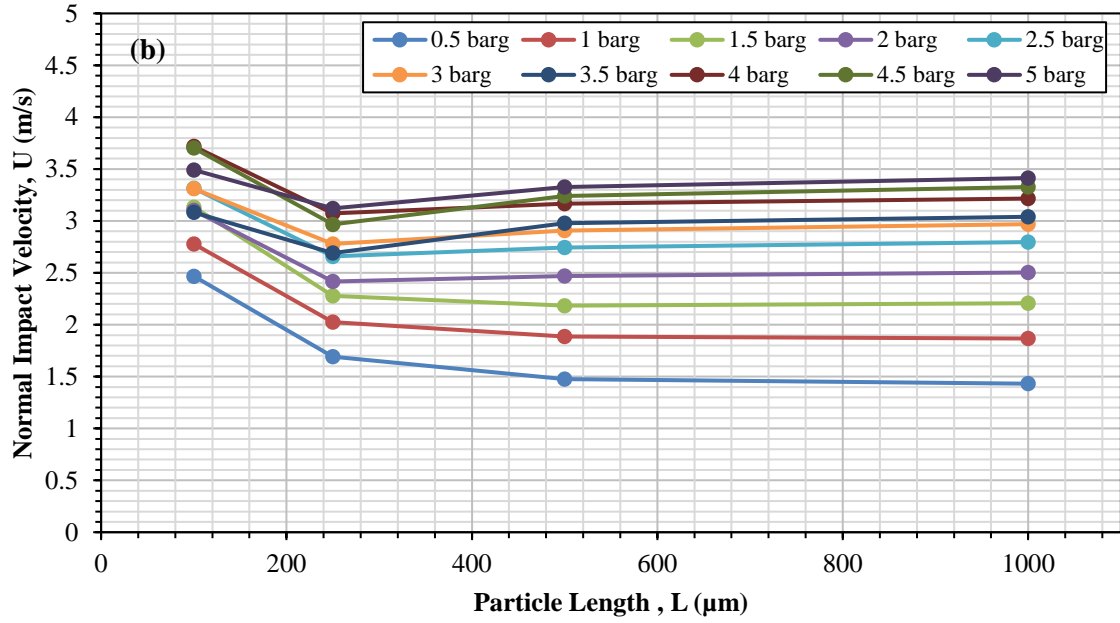
Fig. 8 Extent of breakage of carbamazepine dihydrate crystals at different dispersion pressures



3

4

Fig. 9 Fracture of carbamazepine dihydrate crystal along its width (a) and its length (b)

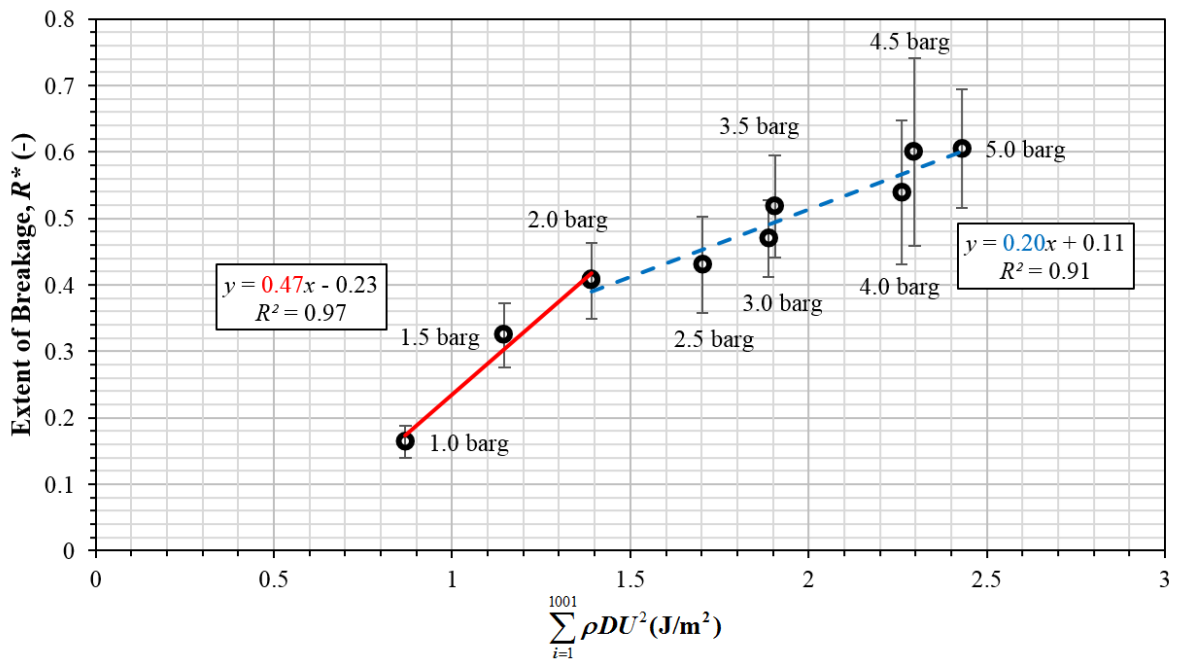


1

Fig. 10 Normal impact velocity of carbamazepine at different dispersion pressure as a function of particle length

2

3



4

5

Fig. 11 Segmented regression of R^* versus $\sum_{i=1}^n \rho D U^2$ (normal impact)